Operando Spectroscopic and Kinetic Characterization of Aerobic Allylic C–H Acetoxylation Catalyzed by $Pd(OAc)_2$/4,5-Diazafluoren-9-one

Jonathan N. Jaworski, Caitlin V. Kozack, Stephen J. Tereniak, Spring Melody M. Knapp, Clark R. Landis,[†] Jeffrey T. Miller,[‡] Shannon S. Stahl[†]*

[†] Department of Chemistry, University of Wisconsin-Madison, 1101 University Avenue Madison, WI, 53706, United States

[‡] David School of Chemical Engineering, Purdue University, 480 Stadium Mall Dr., West Lafayette, IN 47907, United States

RECEIVED DATE

Abstract: Allylic C–H acetoxylations are among the most widely studied palladium(II)-catalyzed C–H oxidation reactions. While the principal reaction steps are well established, key features of the catalytic mechanisms are poorly characterized, including the identity of the turnover-limiting step and the catalyst resting state. Here, we report a mechanistic study of aerobic allylic acetoxylation of allylbenzene with a catalyst system composed of $Pd(OAc)_2$ and 4,5-diazafluoren-9-one (DAF). The DAF ligand is unique in its ability to support aerobic catalytic turnover, even in the absence of benzoquinone or other co-catalysts. Herein, we describe operando spectroscopic analysis of the catalytic reaction using X-ray absorption and NMR spectroscopic methods that allow direct observation of the formation and decay of a palladium(I) species during the reaction. Kinetic studies reveal the presence of two distinct kinetic phases: (1) a burst phase, involving rapid formation of the allylic acetoxylation product and formation of the dimeric Pd^{I} complex $[Pd^{I}(DAF)(OAc)]_2$, followed by (2) a post-burst phase that coincides with evolution of the catalyst resting state from the Pd^{I} dimer into a π-allyl-Pd^{II} species. The data provide unprecedented insights into the

role of ancillary ligands in supporting catalytic turnover with O_2 as the stoichiometric oxidant and establish an important foundation for the development of improved catalysts for allylic oxidation reactions.

Introduction

The Wacker process for industrial production of acetaldehyde from ethylene was discovered in 1959,[1] and three years later Vargaftik et al. reported the first example of Pd^{II}-mediated allylic acetoxylation of olefins.[2] The latter reaction employed stoichiometric $PdCl_2$ in acetic acid and generated linear allyl acetates from terminal olefins, such as 1-hexene. Shortly thereafter, Anderson and Winstein reported allylic acetoxylation of cyclohexene with stoichiometric $Pd(OAc)_2$.[3] In the subsequent half century, extensive efforts were directed toward the development of catalytic methods for this reaction through the combination of Pd^{II} sources with a stoichiometric oxidant capable of promoting reoxidation of Pd^0 to Pd^{II}.[4] The most widely used oxidant is benzoquinone,[2-13] but other oxidants include $CuCl_2$,[14,15] inorganic and organic peroxides,[16-19] and hypervalent iodine reagents.[20,21] Molecular oxygen is also a viable oxidant, typically when used in combination with one or more redox active cocatalysts to facilitate regeneration of the Pd^{II} catalyst.[22-30]

The development of ligand-supported catalyst systems has stimulated renewed interest in Pd-catalyzed allylic oxidation reactions in recent years.[7,8,12,31] These catalyst systems, which contrast the simple Pd^{II} salts [e.g., $PdCl_2$ or $Pd(OAc)_2$] primarily employed as catalysts during the first four decades of the field, facilitate catalyst optimization efforts and introduce new opportunities to achieve catalyst controlled selectivity in the reactions. For example, chelating ligands bearing one or two sulfoxides have been used in reactions that generate branched allyl acetates from terminal olefins,[7,12] rather than the more commonly observed linear allyl acetates. This ligand-controlled regioselectivity has been implemented in a number of synthetic applications,[32-34] and other ligand-

supported catalysts have begun showing promise in enantioselective and diastereoselective reactions.[9,35-38] Ligands can also support more efficient catalysis,[39-41] as revealed by the ability of 4,5-diazafluoren-9-one (DAF) to support aerobic catalytic turnover, even in the absence of redox-active co-catalysts.[31]

In spite of the long history and recent progress, Pd-catalyzed allylic oxidation reactions remain at a relatively early stage of development in comparison to other Pd-catalyzed reactions, with none of the existing catalyst systems exhibiting a full complement of desirable characteristics. For example, catalyst systems that support aerobic catalytic turnover generate only linear allyl acetate products with terminal olefins,[30,31] while catalyst systems that enable branched product formation exhibit relatively poor catalytic performance (e.g., 3-10 turnovers, 48–72 h reaction times) and are not effective with O_2 as the oxidant.[8,12] The mechanistic origin of these limitations is poorly understood. While the basic reaction steps associated with Pd-catalyzed allylic C–H oxidation are well established, few insights are available into the catalytic mechanisms, such as the identity of the turnover limiting step, the composition of the catalyst resting state, and the influence of ancillary ligands on these features. Insights of this type have played a major role in advancing other classes of homogeneous catalytic reactions. For example, Pd-catalyzed cross-coupling methods are some of the most versatile methods in synthetic chemistry. The basic reaction steps involved in these reactions were well established by the early 1970s, but the development of more efficient catalysts, expansion of the synthetic scope and utility, and the emergence of new reaction classes (e.g., Buchwald-Hartwig reactions) in subsequent decades benefitted greatly from mechanistic studies of catalytic reactions.[42-45] For example, insights into the kinetic bottlenecks of the catalytic cycle and characterization of the catalyst species, including on- and off-cycle species,[46-48] provided a foundation for the discovery of new ligands,[49-51] catalyst systems,[52] and

reaction conditions that overcame existing limitations.[53,54] The iterative synergy between empirical and mechanistic studies is much less evident in the field of Pd-catalyzed allylic oxidation reactions; however, the emergence of ligand-supported catalyst systems amenable to this approach is still relatively recent.

Here, we report the first kinetic and mechanistic investigation of a Pd-catalyzed method for aerobic allylic C–H oxidation, focusing on DAF/$Pd(OAc)_2$-catalyzed acetoxylation of allylbenzene, for which the basic steps are illustrated in Scheme 1. The initial report of this catalyst revealed that DAF is unique in its ability to support aerobic catalytic turnover among a series of (bi)pyridyl-based ligands (Scheme 2),[31,55,56] and investigation of stoichiometric reactions with π-allyl-Pd^{II} species showed that DAF promotes reductive elimination[57] of the allyl acetate product.[31,58] The implications of these observations were not extended to catalytic conditions, however, and the present study provides a comprehensive analysis of the catalytic mechanism, including kinetic studies and operando X-ray absorption spectroscopy (XAS) and NMR spectroscopic analysis of the catalytic reaction, which reveal changes in the identity of the turnover limiting step and evolution of the catalyst species during the reaction. The results provide valuable insights into Pd-catalyzed allylic oxidation reactions and the ability of DAF to support aerobic catalytic turnover,[59-69] and this study establishes an important foundation for future empirical and mechanistic efforts directed toward the identification of more efficient and synthetically useful allylic C–H oxidation catalyst systems.

Scheme 1. Proposed Mechanism for DAF-Promoted Pd-Catalyzed Aerobic Acetoxylation.

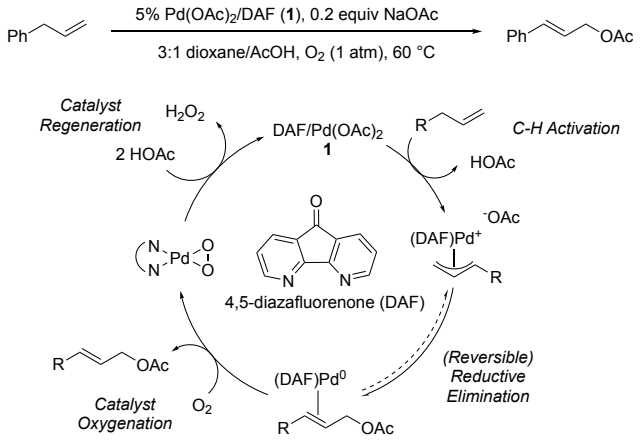

Scheme 2. DAF-Promoted Pd-Catalyzed Aerobic Allylic Acetoxylation of Alkenes.[31]

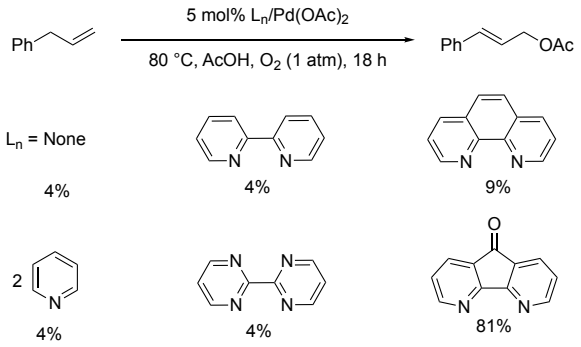

Results and Discussion

Initial mechanistic observations. In a recent study, we showed that DAF/$Pd(OAc)_2$-catalyzed allylic acetoxylation of allylbenzene exhibits a kinetic burst at the beginning of the reaction and generates a dimeric Pd^I species under the catalytic conditions.[70] These preliminary results, reproduced in Figure 1, provided a starting point for the present investigation, with the goal of understanding the origin and implications of these observations. The burst is accompanied by a change in the color of the reaction solution from yellow to red, but, as the reaction progresses past the burst, the reaction solution changes color again from red to yellow. The latter color persists for the remainder of the reaction.[71] A red Pd^I dimer, $[Pd^I(DAF)(OAc)]_2$ **2**, was independently

synthesized and characterized by X-ray crystallography (Figure 1B), and it exhibits a UV-visible absorption spectrum that closely matches the UV-vis spectra observed from the catalytic reaction mixture (Figure 1C).[70]

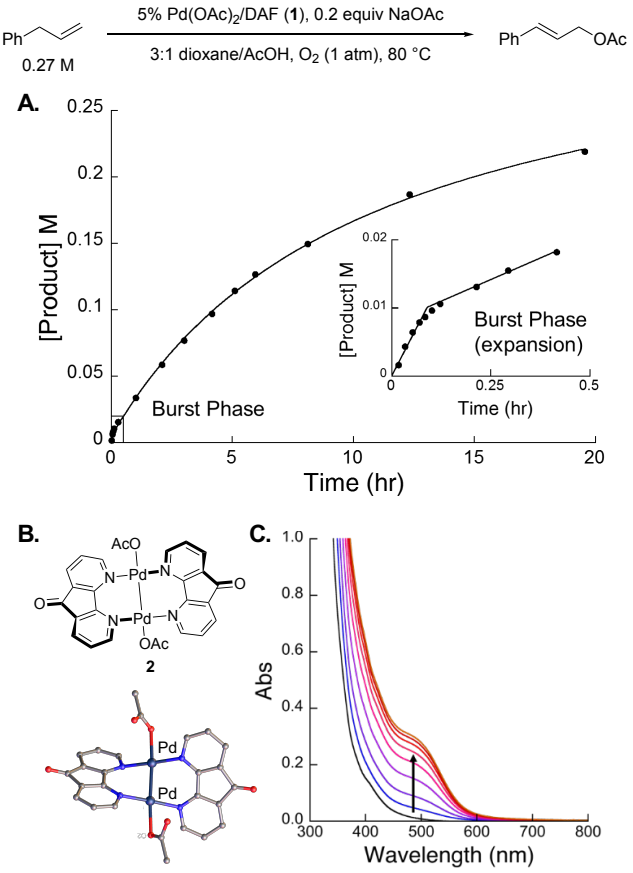

Figure 1. Previous observations from allylic acetoxylation of allylbenzene catalyzed by DAF/$Pd(OAc)_2$. (A) Time course of the acetoxylation reaction at 80 °C. (B) Drawing and X-ray crystal structure of the Pd^I dimer, $[Pd^I(DAF)(OAc)]_2$ **2**. (C) UV-vis absorption spectra obtained during the burst phase of the catalytic reaction. Figures adapted with permission from ref. 70. Copyright 2017 John Wiley & Sons, Inc.

Interrogation of the catalyst speciation by X-ray absorption spectroscopy. The data noted above imply that the oxidation state of the Pd catalyst changes during the course of the reaction. Palladium K-edge X-ray absorption spectroscopy probes the excitation of Pd 1s electrons, and the "near edge" absorption energy, corresponding to the 1s → 5p orbital transition, provides insight

into the oxidation state of Pd complexes.[72,73] This technique has been used to probe a number of homogeneous Pd-catalyzed reactions,[74-79] including recent analysis of a Pd-catalyzed aerobic oxidation of an aromatic C–H bond.[80] In order to conduct analogous experiments for the allylic acetoxylation reaction, a reactor was designed and constructed to enable operando studies on the high photon-flux beamline at Argonne National Laboratories (see Supporting Information for details; Figures S3–S6).

Pd K-edge XANES spectra were obtained for a series of Pd^0, Pd^I, and Pd^{II} reference compounds: Pd^0 ($Pd_2(dba)_3$), Pd^I ($[Pd^I(DAF)(OAc)]_2$ (**2**)), and Pd^{II} (1:1 DAF/$Pd(OAc)_2$ (**1**); $[Pd^{II}(\pi\text{-cinnamyl})(OAc)]_2$ (**3**); and $[Pd^{II}(DAF)(\pi\text{-cinnamyl})]BF_4$ (**4**)). Similar spectra were then acquired during the course of the catalytic reaction,[81] with a time course of the edge energy shown together with selected reference compounds in Figure 2A. Upon initiation of the reaction by injecting allylbenzene, the edge energy shifts rapidly from its initial position associated with **1** to a lower energy position, consistent with reduction of the catalyst during the burst (spectrum **B**). The new edge energy is very similar to that of the Pd^I dimer reference (cf. **2**, Figure 2B). Analysis of the extended X-ray absorption fine-structure (EXAFS) region of the spectra revealed three prominent scattering peaks during the first 13 min of the reaction, and these peaks are very similar to those observed with an authentic sample of the Pd^I dimer **2** (Figure 3A). Collectively, the XANES and EXAFS spectra support the formation of Pd^I species **2** as a catalytic intermediate during the burst phase of the reaction.

As the reaction proceeds, the edge increases gradually to higher energy, ultimately reaching an energy intermediate between that of DAF/$Pd^{II}(OAc)_2$ **1** and the Pd^I dimer **2** (Figure 2A). An

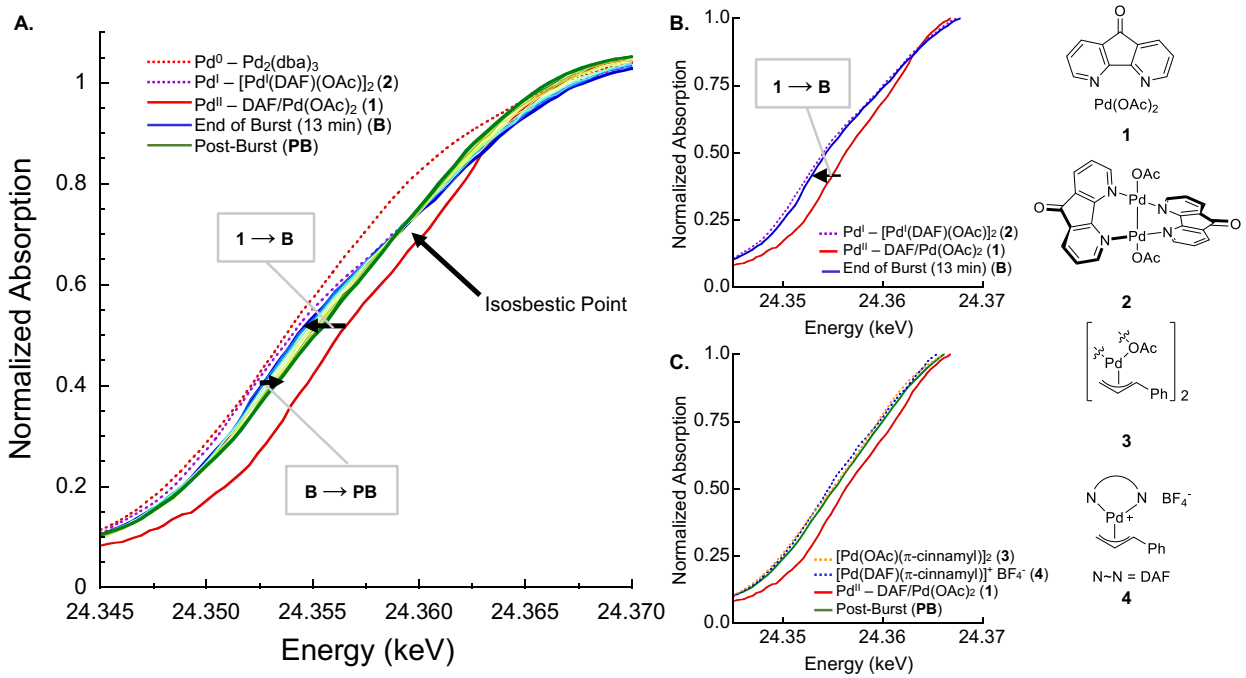

Figure 2. XAS K-edge analysis of Pd reference compounds and the catalyst during the allylic oxidation reaction (note: "B" refers to the "burst" phase and "PB" refers to the "post-burst" phase of the reaction). (A) Operando Pd K-edge time course overlay from 13-110 minutes with overlaid references for comparison. (B) Operando Pd K-edge time course overlay of 0 and 13 minutes with comparison of $[Pd^{I}(DAF)(OAc)]_2$ (**2**) reference. (C) Comparison of the post-burst with neutral π-allyl Pd^{II} acetate dimer, $[Pd^{II}(\pi\text{-cinnamyl})(OAc)]_2$ (**3**) and cationic π-allyl Pd^{II} monomer, $[Pd^{II}(DAF)(\pi\text{–cinnamyl})]BF_4$ (**4**). The catalytic reaction was carried out on a 3 mL scale in 3:1 dioxane:AcOH where [allylbenzene] = 0.27 M, [NaOAc] = 0.54 mM, and $[DAF/Pd(OAc)_2]$ = 13.5 mM in a PEEK cell with an O_2 balloon.

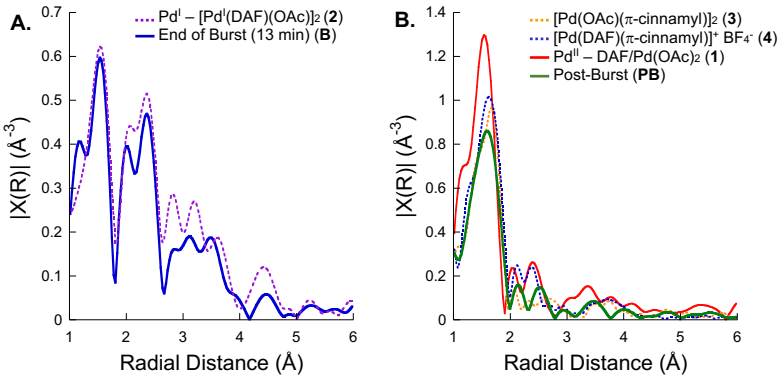

Figure 3. Operando EXAFS k^2-weighted four transforms at t = 13 min and post-burst turnover. (**A**) Comparison of the EXAFS at t = 13 min and Pd^{I} dimer $[Pd^{I}(DAF)(OAc)]_2$ (**2**) reference. (**B**) Comparison of the EXAFS from the post-burst period of the catalytic reaction with $DAF/Pd(OAc)_2$ (**1**) and the π-allyl-Pd^{II} reference compounds (**3**) and (**4**). The catalytic reaction was carried out on a 3 mL scale in 3:1 dioxane:AcOH where [allylbenzene] = 0.27 M, [NaOAc] = 0.54 mM, and $[DAF/Pd(OAc)_2]$ = 13.5 mM in a PEEK cell with an O_2 balloon.

isosbestic point is evident in the XANES spectra during this phase of the reaction (cf. Figure 2A), suggesting that the Pd^{I} dimer converts directly into a new Pd species, which has a higher formal oxidation state. The XANES spectrum for the catalyst resting state in the post-burst phase (**PB**) is clearly different from the DAF/$Pd^{II}(OAc)_2$ pre-catalyst **1**, and it closely resembles the spectra of the independently prepared π-allyl-Pd^{II} species, the dimeric species $[Pd^{II}(\pi\text{-cinnamyl})(OAc)]_2$ (**3**) and the monomeric DAF-ligated π-allyl-Pd^{II} species, $[Pd^{II}(DAF)(\pi\text{-cinnamyl})]BF_4$ (**4**) (Figure 2C). The changes evident in the XANES spectra were also evident in a comparison of the inflection point in the spectra for the Pd species present during the reaction relative to the approximate edge energies of the Pd^{I} and Pd^{II} reference compounds (Figure 4). Analysis of the EXAFS spectral region during the post-burst portion of the reaction also reveal similarities between the post-burst Pd^{II} intermediate (**PB**) and the π-allyl-Pd^{II} reference compounds (Figure 3B).

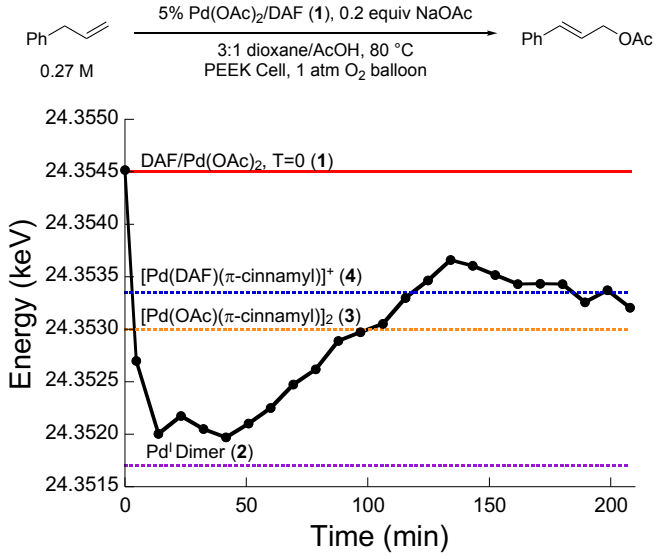

Figure 4. Time course plot of the XANES edge energy of the Pd catalyst during the catalytic allylic acetoxylation reaction, relative to the edge energies corresponding to well-defined Pd reference compounds.

Interrogation of catalyst speciation by NMR spectroscopy. The catalyst speciation during the reaction time course was also interrogated by NMR spectroscopic methods. The reaction

employs a mixture of AcOH/NaOAc as the solvent and source of acetate nucleophile, and the predominant palladium species observed by ^{1}H NMR spectroscopy at the start of the reaction was identified as an "ate" complex, Na[(κ^1-DAF)$Pd^{II}(OAc)_3$] (**5**). This assignment was supported by NMR integrations and independent titration studies involving addition of NaOAc to a solution of DAF and $Pd^{II}(OAc)_2$ (Figures S20-S24). A time course of the reaction was monitored by ^{1}H NMR spectroscopy by using a sealed NMR tube pressurized with 3.2 atm of static O_2. The data reveal rapid product formation with concurrent conversion of the Pd^{II} ate complex **5** into the Pd^{I} dimer **2** (Figure 5). The concentration of Pd^{I} maximizes at the end of the kinetic burst of product formation (t ~ 20 min), after which the rate of cinnamyl acetate product formation decreases to a steady-state rate. Unligated DAF becomes evident in the reaction mixture and its concentration increases during the steady state reaction period (Figure 5 - expansion).

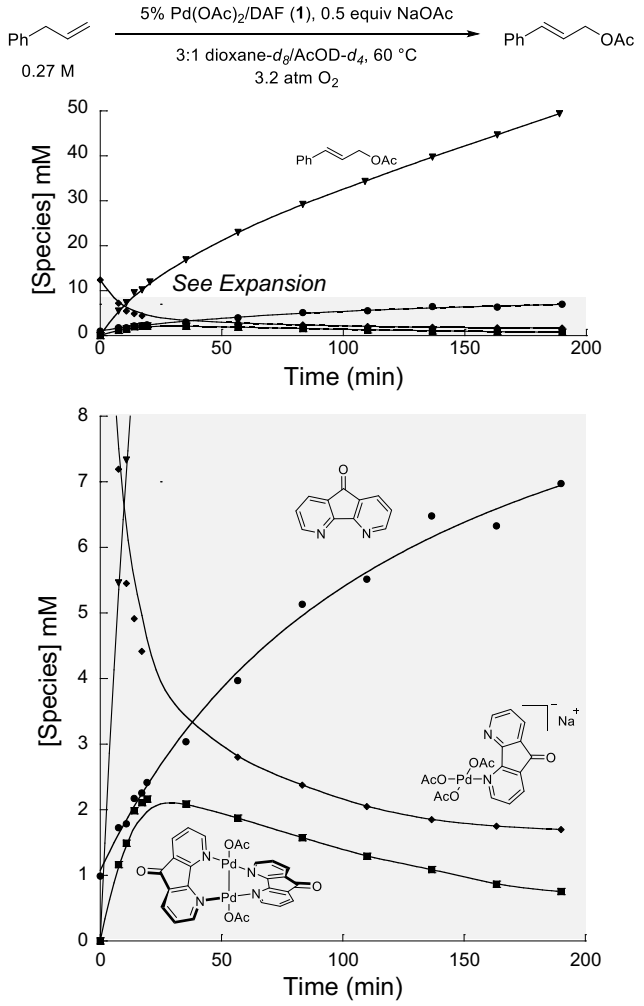

Figure 5. Initial investigations into the resting state of the catalyst as followed by an NMR time course of product formation and DAF speciation with 3.2 atm static O_2 at 60 °C and expansion of DAF speciation in the NMR time course. Lines reflect smooth fits to the data to guide the eye.

To investigate the catalyst speciation at early reaction times (i.e., during the burst period), thick-walled NMR tubes were prepared with different pressures of O_2.[82-84] Plots showing the formation of cinnamyl acetate and the Pd^I dimer (**2**) at 0.2-6.2 atm O_2 are provided in Figure 6. Nearly identical rates of product formation (i.e., independent of the pO_2) are evident during the burst phase; however, the rate of product formation after the burst phase increases with increasing pO_2 (Figure 6A). Complementary analysis of the Pd species shows that the amount of Pd^I dimer **2**

generated during the burst phase decreases with increasing pO_2 (Figure 6B; see Supporting Information for further details).

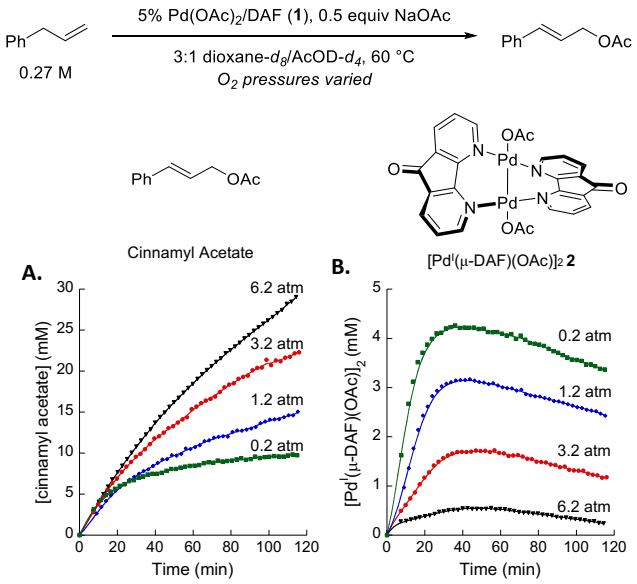

Figure 6. Time courses with different initial pressures of O_2 (static) monitored by NMR spectroscopy. Conditions: [DAF] = 13.5 mM, [$Pd(OAc)_2$] = 13.5 mM, [allylbenzene] = 0.27 M, [NaOAc] = 54 mM, 60 °C. (A) [cinnamyl acetate] over time at pO_2 = 0.2 to 6.2 atm. (B) [[Pd^I(μ-DAF)(OAc)]$_2$] over time at pO_2 = 0.2 to 6.2 atm. Lines reflect a smooth fit to the data to guide the eye.

To complement these data, the recently developed Wisconsin High Pressure NMR Reactor (WiHP-NMRR)[85-87] was used to monitor the dependence of the rate on O_2 pressure (pO_2). This apparatus provides continuous gas circulation in the liquid during the NMR relaxation delay (d1). This dynamic gas supply allows for better control of dissolved O_2 concentration during the reaction and avoiding complications that can arise from the lack of gas-liquid mixing in an NMR tube when a static pressure of O_2 is used.[88] Consistent with the data in Figure 6, the rate of product formation during the burst phase was not affected by changes in pO_2, while a saturation dependence of the rate on pO_2 was evident from kinetic data after the burst (Figure 7).

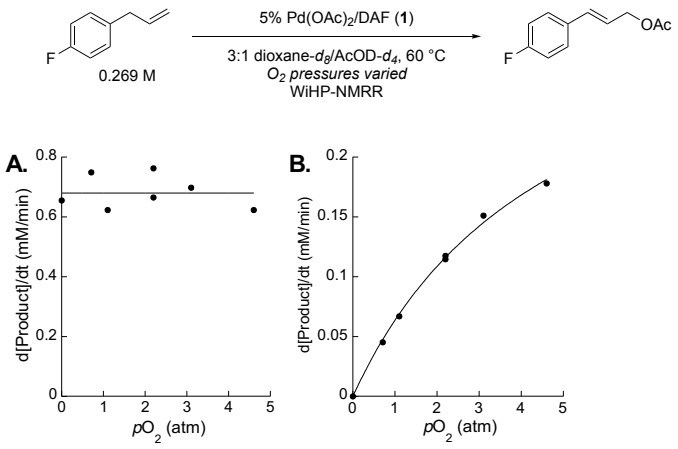

Figure 7. Dependence of the rate of allylic acetoxylation on pO_2 (dynamic) during (A) burst and (B) post-burst phase of the reaction. Conditions: [DAF/$Pd^{II}(OAc)_2$] = 13.5 mM, [4-fluoroallylbenzene] = 0.27 M, 0–4.6 atm pO_2 using 9% O_2 in N_2, 60 °C; NaOAc was not used in order to prevent clogging of the gas inlet capillary. ds = 0, ns = 2, d1 = 4s, circulation delay between scans = 0.5 s, aq = 0.3 s. The line in (B) reflects a smooth fit to the data to guide the eye.

Another set of studies was conducted to probe the influence of substrate concentration on the reaction rate and Pd speciation during the early periods of the reaction (0.135–1.08 M allylbenzene). The overall rate of product formation increased with higher [allylbenzene] (Figure 8A). An increase in the rates of formation and decay of the Pd^{I} dimer **2** with increasing [allylbenzene] results in a similar maximum concentration of **2** under all conditions, but a shorter lifetime for this species at higher substrate concentration (Figure 8B).

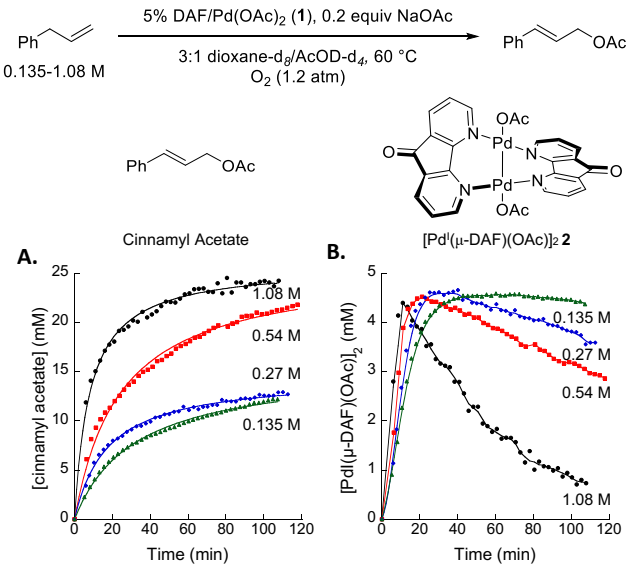

Figure 8. Time courses with different concentrations of allylbenzene monitored by NMR spectroscopy under static O_2 pressure. Conditions: [DAF] = 13.5 mM, [$Pd(OAc)_2$] = 13.5 mM, [allylbenzene] = 0.135-1.08 M, [NaOAc] = 54 mM, 60 °C, 1.2 atm O_2 (static). (A) [cinnamyl acetate] over time. (B) [[Pd^{I}(μ-DAF)(OAc)]$_2$] over time. Lines reflect a smooth fit to the data to guide the eye.

Kinetic studies and isotope effects. More thorough kinetic studies were performed to probe the contributions of each of the reaction components to the reaction rate during the burst and post-burst phases of the reaction (Figures 9 and 10). These studies were conducted at 40 °C and 80 °C, respectively, by removing aliquots of the reaction mixture and analyzing product formation by gas chromatography (GC). Analysis of the burst phase was carried out at lower temperature to enable acquisition of more precise data, but the results are consistent with general trends observed at higher temperatures. A linear dependence of the rate on the 1:1 DAF/$Pd^{II}(OAc)_2$ catalyst concentration [**1**] was observed during the burst phase, while a slight saturation dependence was evident in the post-burst regime (Figures 9A and 10A, respectively). In both the burst and post-burst phases, the rate exhibits a nearly linear dependence on [DAF] up to a 1:1 DAF/$Pd^{II}(OAc)_2$ ratio; however, increasing [DAF] beyond a 1:1 ratio decreases the rate of the burst, while it does not affect the rate during post-burst turnover (Figures 9B and 10B). A nearly linear dependence on

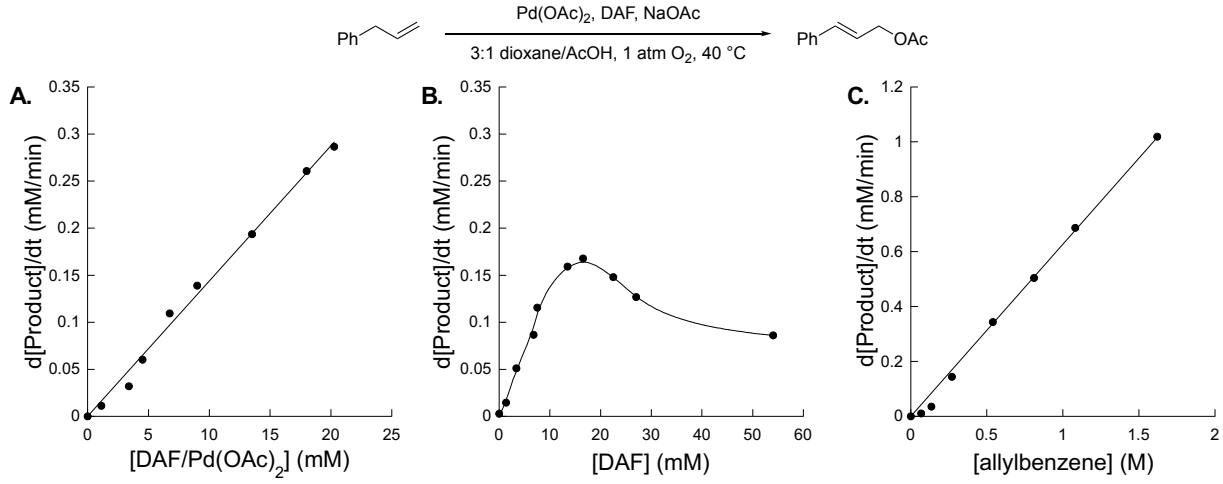

Figure 9. Kinetic dependencies of reaction components for the burst phase. All experiments were performed at 40 °C in an orbital mixer with 1 atm of O_2 and 54 mM NaOAc. (A) [DAF] = [$Pd(OAc)_2$] = 0-18 mM, [allylbenzene] = 0.27 M. (B) [DAF] = 0-54 mM, [$Pd(OAc)_2$] = 13.5 mM, [allylbenzene] = 0.27 M. (C) [DAF/$Pd^{II}(OAc)_2$] = 13.5 mM, [allylbenzene] = 0.14-1.8 M. Average of multiple runs. Error within 10%. The line in (B) reflects a smooth fit to the data to guide the eye.

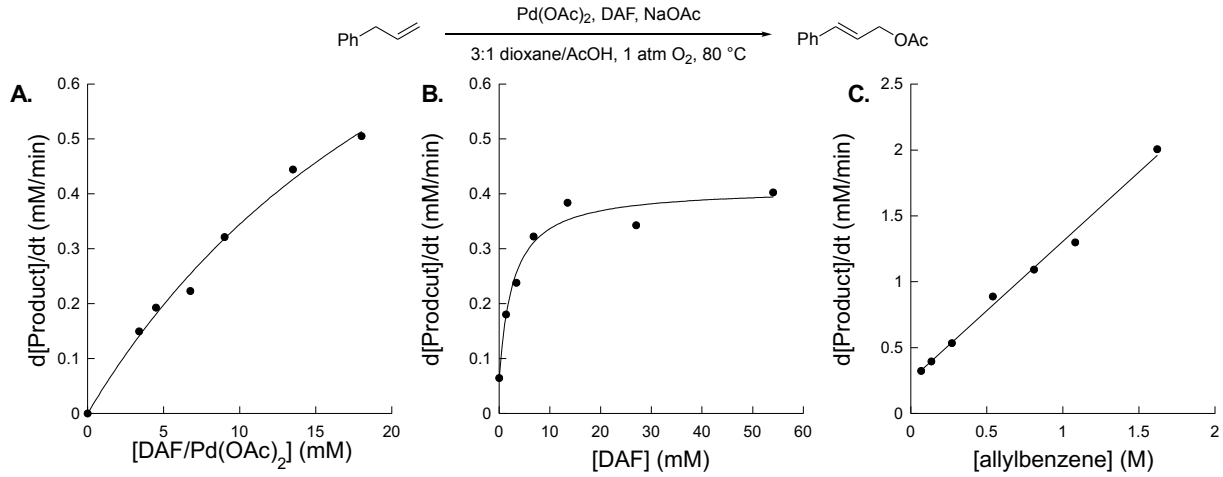

Figure 10. Kinetic dependencies of reaction components after the burst phases of the reaction. All experiments were performed at 80 °C in an orbital mixer with 1 atm of O_2 and 54 mM NaOAc. (A) [DAF/$Pd^{II}(OAc)_2$] = 0-18 mM, [allylbenzene] = 0.27 M. (B) [DAF] = 0-54 mM, [$Pd(OAc)_2$] = 13.5 mM, [allylbenzene] = 0.27 M. (C) [DAF/$Pd^{II}(OAc)_2$] = 13.5 mM, [allylbenzene] = 0.14-1.8 M. Average of multiple runs. Error within 10%. The lines for (A) and (B) represents a hyperbolic fit to the data, i.e., rate = $c_1 \cdot x / (c_2 + c_3 \cdot x)$, with a non-zero intercept for (B).

[allylbenzene] was observed in the burst and post-burst phases (Figures 9C and 10C), but the data intersect at the origin for the burst kinetics, while the post-burst kinetic data exhibit a substantial

non-zero intercept. The positive order in [allylbenzene] in both cases correlates with the kinetic influence of allylbenzene on the rate of formation and decay of the Pd^{I} dimer **2** observed in the NMR spectroscopic studies shown in Figure 8B.

Two deuterium-labeled substrates were synthesized to probe intramolecular and intermolecular kinetic isotope effects (KIEs). 4-Allylbiphenyl (**6**) was selected as the substrate for these studies because it is not volatile and is easier to purify than the parent allylbenzene.[89] Independent rates were measured with **6** and **6**-d_2 substrates, and intramolecular competition KIEs with **6**-d_1 were determined via ^{1}H NMR spectroscopy by quantifying the product formation derived from C–H or C–D activation. The primary KIEs evident in the burst phase from both sets of experiments (Table 1, entries 1 and 2) are rather small, but very similar to that observed in a recent allylic amination reaction.[90] In the period of the reaction after the burst, the intramolecular competition experiment revealed a KIE similar to that observed in the burst phase (cf. entry 3 vs entries 1 and 2), but essentially no KIE was observed from the independent rate measurements (entry 4).

Table 1. Kinetic Isotope Effects Obtained via Independent Rate Measurements with **6**/**6**-d_2-Labeled Substrates and via Intramolecular Competition Using the **6**-d_1-Labeled Substrate.

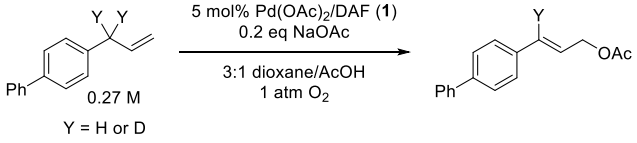

Temp	Phase	Experiment	KIE
40 °C	Burst	Intramol. Competition (**6**-d_1)	1.5 ± 0.4
		Independent Rate (**6**, **6**-d_2)	1.6 ± 0.1
80 °C	Post-Burst	Intramol. Competition (**6**-d_1)	1.6 ± 0.2
		Independent Rate (**6**, **6**-d_2)	1.05 ± 0.03

Evolution of a π-cinnamyl-Pd^{II} resting state following the burst. The XAS data described above implicate the possibility of a π-allyl-Pd^{II} species as the catalyst resting state during the post-burst phase of the reaction. Initial attempts to observe such a species directly by ^{1}H NMR spectroscopy were unsuccessful, however, possibly reflecting a high degree of fluxionality associated with such a species.[91-93] The NMR time course in Figure 5 suggests that the DAF ligand dissociates from the Pd center during the reaction, a feature that could further contribute to the fluxionality of a π-allyl-Pd^{II} species and complicate its detection by ^{1}H NMR spectroscopy.

To overcome this complication, we analyzed the catalytic acetoxylation of 4-fluoroallylbenzene to probe the reaction by ^{19}F NMR spectroscopy. Operando analysis of the catalytic reaction was conducted throughout the time course using the WiHP-NMRR in an effort to identify possible intermediates. During the burst phase, ^{19}F NMR resonances are evident only for the alkene starting material (-113.4 ppm) and cinnamyl acetate product (-110 ppm) (e.g., Figure 11a). As the reaction proceeds, however, a new resonance becomes evident at -109.2 ppm. (Figure 11b; see Figure S12 for additional spectra). The chemical shift of this peak, denoted **I**, is very similar that observed from an independently prepared sample of the 4-fluorophenyl derivative of the π-cinnamyl-Pd^{II} dimer **3** (i.e., **3**^{F}) and the same compound in the presence of DAF (DAF:Pd = 1:1) (Figures 11c and 11d). Integration of this resonance during the course of the catalytic reaction show that this species accounts for nearly all of the Pd catalyst present in solution (Figure 12), thereby providing direct support for evolution of the catalyst into a π-allyl-Pd^{II} resting state following the burst.

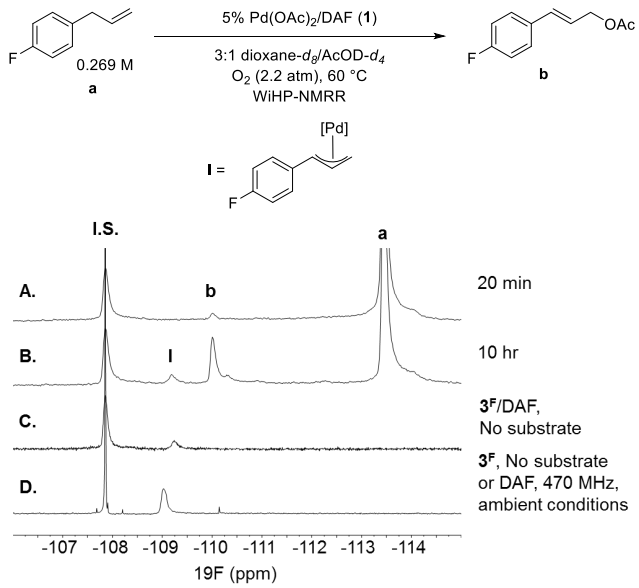

Figure 11. In situ detection of a π-cinnamyl-Pd^{II} resting state during the acetoxylation of 4-fluoroallylbenzene using the WiHP-NMRR. $Pd(OAc)_2$ as precatalyst, (A) 20 min and (B) 10 h after reaction initiation, $\mathbf{3^F}$/DAF without substrate (C), and $\mathbf{3^F}$ under ambient conditions without other reaction components (D). Conditions: [Pd] = 13.5 mM, [DAF] = 13.5 mM (except for the bottom spectrum, where [DAF] = 0), 3-fluoroanisole internal standard. [I.S.] = 55.7 mM, 3:1 dioxane:AcOD-d_4.

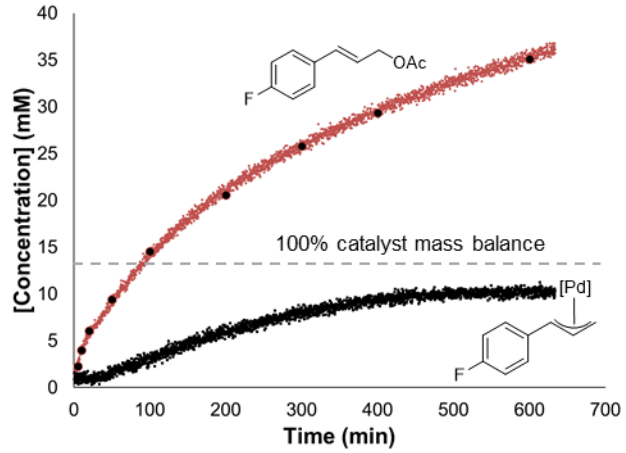

Figure 12. Time course of DAF/$Pd^{II}(OAc)_2$-catalyzed allylic acetoxylation of 4-fluoroallylbenzene analyzed by ^{19}F NMR spectroscopy using the WiHP-NMRR. See Figure 11 for reaction conditions. The superimposed points in the red data correspond to the representative NMR spectra depicted in the Supporting Information, Figure S12.

In light of these observations, the initial time course of the catalytic acetoxylation of allylbenzene was analyzed by comparing reactions conducted with $Pd(OAc)_2$ and [Pd^{II}(π-cinnamyl)(OAc)]$_2$ (**3**) as the source of Pd catalyst, under otherwise identical conditions. The data

in Figure 13 show that no burst is observed when **3** is used as the Pd precatalyst, and the initial rate in this reaction resembles that of the post-burst rate observed from the reaction initiated with $Pd(OAc)_2$ as the precatalyst.

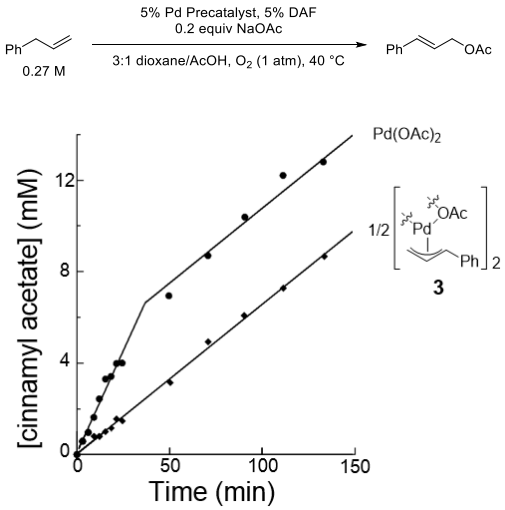

Figure 13. Kinetic interrogation of the resting state. Pd precatalyst = DAF/$Pd^{II}(OAc)_2$ **1** or $[Pd^{II}(\pi\text{-cinnamyl})(OAc)]_2$ **3**.

Investigation of allyl acetate reductive elimination from $[Pd^{II}(\pi\text{-cinnamyl})(OAc)]_2$. Identification of a π-allyl-Pd^{II} resting state during the catalytic reaction prompted us to prepare the well-defined $[Pd^{II}(\pi\text{-cinnamyl})(OAc)]_2$ species **3** to explore its reactivity under catalytically relevant conditions (Figure 14). As a control experiment, negligible reductive elimination of cinnamyl acetate[57] was observed under N_2 in the absence of the DAF ligand (Figure 14, condition *a*). Some reactivity was observed upon addition of DAF to the solution of **3** under N_2 (condition *b*), consistent with previously reported observations,[31] and further enhancement of the reaction was observed upon adding an equivalent of DAF/$Pd^{II}(OAc)_2$ (condition *c*). The latter conditions led to significant formation of the Pd^{I} dimer **2**. These reactions were also enhanced by conducting the reaction under an atmosphere of O_2 (conditions *d* and *e*). The last of these conditions (*e*) resemble the reaction conditions present during the burst phase of the catalytic reaction, when

allylic C–H activation and formation of an allyl-Pd^{II} intermediate will take place in the presence of additional DAF/$Pd^{II}(OAc)_2$ pre-catalyst, which can react with the Pd^0 species formed upon reductive elimination of cinnamyl acetate and generate the Pd^I dimer **2** (see further discussion below). The presence of allylbenzene has negligible effect on the rate of reductive elimination (see Figure S17 in the Supporting Information), suggesting that the beneficial kinetic effect of allylbenzene after the burst (cf. Figure 10C) does not arise from the reductive elimination step, but rather from its contribution to catalyst speciation (i.e., by promoting conversion of Pd^I dimer **2** into the steady-state Pd^{II} catalyst; cf. Figure 8B).

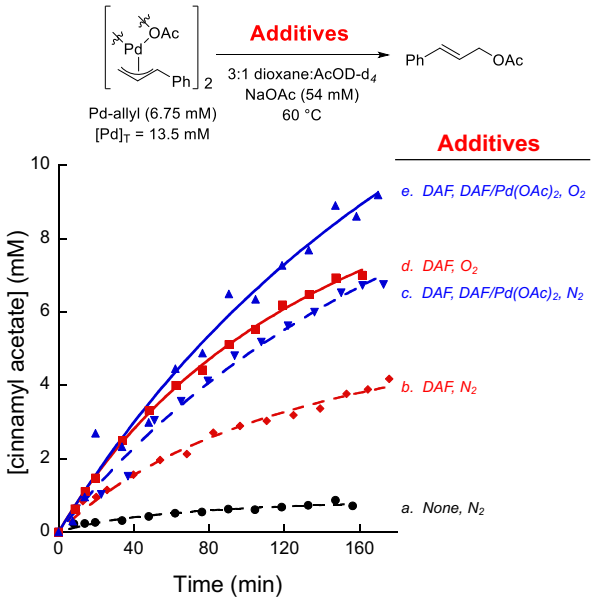

Figure 14. Stoichiometric reductive elimination reactions of $[Pd^{II}(\pi\text{-cinnamyl})(OAc)]_2$. Conditions: $[Pd^{II}(\text{cinnamyl})(OAc)]_2$ = 6.75 mM, [DAF] = 13.5 mM, [DAF/$Pd(OAc)_2$] = 13.5 mM, [NaOAc] = 54 mM, 60 °C, 3:1 dioxane:AcOD-d_4, N_2 or O_2. The lines reflect smooth fits to the data to guide the eye.

Catalytic mechanism: Overview of observations. The data presented above provide key insights into the DAF/$Pd^{II}(OAc)_2$-catalyzed acetoxylation of allylic C–H bonds, including factors that affect the rate of the reaction and the identity of the catalyst resting state (Table 2). Briefly,

the kinetic burst phase evident at the beginning of the reaction is characterized by a primary deuterium KIE (independent rate measurement) and a lack of rate-dependence on pO_2, and the Pd catalyst evolves from a DAF-ligated Pd^{II}-acetate species into a DAF-bridged Pd^{I} dimer. The ensuing post-burst phase lacks a primary KIE, exhibits a rate-dependence on pO_2, and the Pd catalyst resting state evolves from the DAF-bridged Pd^{I} dimer into π-allyl-Pd^{II} species with bound and unbound DAF ligand.

Table 2. Summary of the Mechanistic Observations for the Burst and Post-Burst Regimes.

	Burst	**Post-Burst**
Primary Allylic C–H KIE	Yes	No
pO_2 Dependence	No	Yes
DAF Speciation	DAF ligated to Pd^{II} *or* Pd^{I}	Appearance of free DAF
Catalyst Evolution	DAF/Pd^{II} → Pd^{I} dimer	Pd^{I} dimer → π-allyl-Pd^{II} species
Turnover-Limiting Step	C–H activation	Pd^{0} oxidation by O_2

Analysis of the burst phase of the reaction. The deuterium kinetic isotope effect observed during the burst supports allylic C–H activation as the rate-limiting step during this phase.[90,94,95] The resulting allyl-Pd^{II} intermediate undergoes reductive elimination of cinnamyl acetate to afford a Pd^{0} species that reacts with a DAF/$Pd^{II}(OAc)_2$ species to afford the Pd^{I} dimer **2** (Scheme 3; cf. Figure 14). The mechanistic details of reduction elimination and Pd^{II}/Pd^{0} comproportionation steps are not well understood and warrant attention in future studies, but formation of analogous dimeric Pd^{I} species has been studied extensively in Pd-catalyzed cross-coupling reactions.[52,96] Pd^{I} species have also been identified in oxidative carbonylation reactions,[97-100] but the DAF-ligated dimer **2**

represents the first example of a Pd^{I} intermediate identified in ligand-supported Pd-catalyzed aerobic oxidation reactions.[70] A second example was recently reported by Albéniz and Maseras, who detected a Pd^{I} dimer in the aerobic oxidative homocoupling of alkynes with Ph_3P as an ancillary ligand.[101] The use of Pd^{I} dimers as air-stable catalyst precursors in many non-oxidative coupling reactions reactions[52] raises prospects for similar opportunities in aerobic oxidation reactions.

Scheme 3. Mechanism of the Burst Phase of DAF/$Pd^{II}(OAc)_2$-Catalyzed Allylic Acetoxylation.

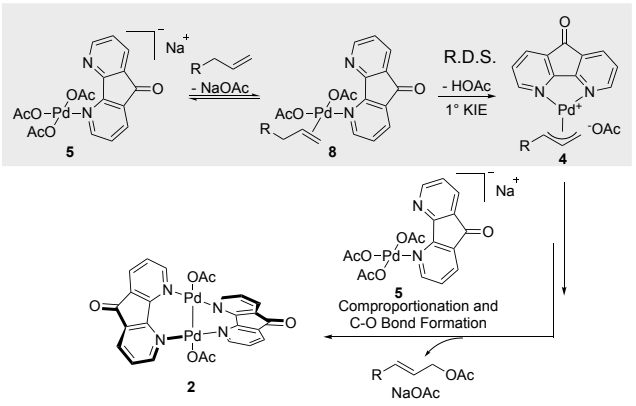

Analysis of the post-burst phase of the reaction. The burst phase concludes as DAF-ligated Pd^{II}-acetate species are depleted and the Pd^{I} dimer concentration reaches a maximum. The collection of kinetic and spectroscopic insights obtained from the reaction following the burst are incorporated into the overall catalytic mechanism proposed in Scheme 4. Previous studies have shown that the Pd^{I} dimer can undergo oxidation to a DAF/Pd^{II}-acetate species in the presence of O_2,[70,102] and the NMR data in Figure 10 show that allylbenzene promotes the conversion of Pd^{I} dimer into a new Pd^{II} form of the catalyst, identified as the allyl-Pd^{II} species **3** (cf. Figure 12),

Scheme 4. Full Mechanism of DAF/$Pd^{II}(OAc)_2$-Catalyzed Allylic Acetoxylation, Including the Burst and Post-Burst Phases of the Reaction.

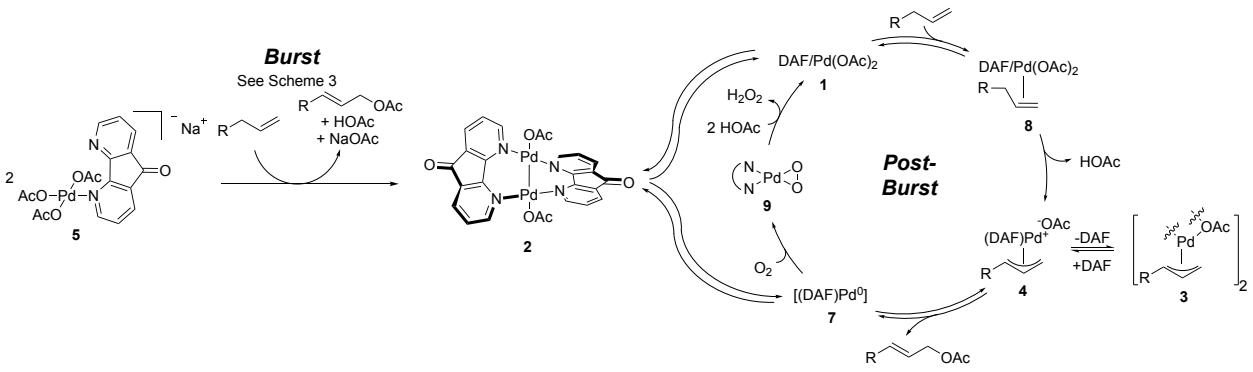

which serves as the catalyst resting state following the burst. This structure is consistent with the appearance of free DAF ligand under these conditions. The stoichiometric reactivity studies with **3**, depicted in Figure 14, show that reductive elimination of cinnamyl acetate[57] is promoted by DAF, O_2, and DAF/$Pd(OAc)_2$; however, following the burst, excess DAF/$Pd(OAc)_2$ species are no longer available in the reaction mixture to promote reductive elimination. This difference between the burst and post-burst conditions rationalizes the change in catalyst speciation and turnover-limiting steps (cf. Table 2). These changes, in turn, account for the lack of a deuterium KIE for C–H activation during the post-burst phase of the reaction and the similarity between the of post-burst turnover rate and the rate of the reaction when π-allyl-Pd^{II} dimer **3** is used as the pre-catalyst (cf. Figure 13).

DAF plays an important role in supporting catalytic turnover under steady-state (post-burst) conditions by facilitating reductive elimination of cinnamyl acetate from the allyl-Pd^{II} species. DAF coordination to the allyl-Pd^{II} dimer **3** is proposed to generate the monomeric DAF-ligated allyl-Pd^{II} species **4**, which can undergo reversible formation of cinnamyl acetate (Figure 15).[31,58] This reaction is driven by trapping of Pd^0 (**7**) by O_2, which is proposed to be the turnover limiting step during this phase of the reaction (Table 2).[103,104] No build-up of Pd^I dimer **2** is observed after

the burst phase due to the low steady-state concentration of the DAF/Pd^{II}-acetate species available to trap Pd^0 species generated in the reductive elimination step. The reaction of O_2 with the Pd^0 species **7** is proposed to proceed in a manner similar to previously reported reactions between O_2 and related well-defined nitrogen-chelated Pd^0 model complexes.[41,105-107]

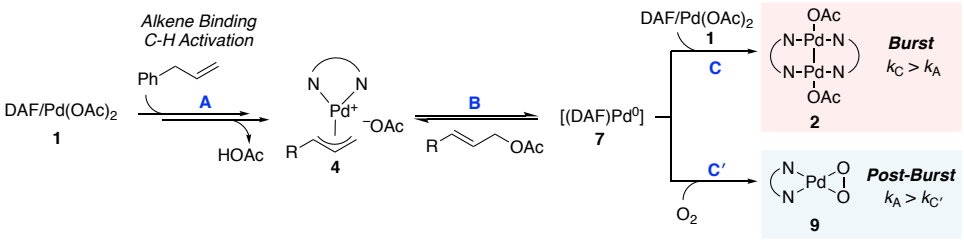

Figure 15. Reaction scheme depicting trapping of Pd^0 by Pd^{II} (**1**) or by O_2 during the burst and post-burst phases of the reaction, with concurrent changes in the rate determining step of the reaction.

As noted in the Introduction, very few mechanistic studies of Pd-catalyzed allylic oxidation reactions have been reported. The two most thorough precedents were reported recently by the groups of Labinger/Bercaw[10] and Fristrup,[94] and focused on bipyrimidine (bpym)/$Pd^{II}(OAc)_2$ and bis(sulfoxide)/$Pd^{II}(OAc)_2$ catalyst systems, respectively. The turnover-limiting step in the former reaction was identified as alkene binding to (bpym)$Pd^{II}(OAc)_2$, while the latter reaction was attributed to C–H activation. The presence of a π-allyl-Pd^{II} catalyst resting state and turnover-limiting reductive elimination are unprecedented, and these two observations likely reflect the use of O_2, rather than benzoquinone, as the stoichiometric oxidant. Benzoquinone was used as the stoichiometric oxidant in both of the previously studied catalytic reactions, and it is known to promote reductive elimination from π-allyl-Pd^{II} species.[7,58,108,109] These considerations highlight opportunities for the development of improved catalyst systems and/or ligand designs that support

more effective reductive elimination while also enabling efficient reaction of Pd^0 with O_2. Efforts toward this end have been initiated.

Conclusion.

This study has implemented a number of different experimental approaches to gain insights into a Pd-catalyzed allylic oxidation reaction that is capable of using O_2 as the stoichiometric oxidant due to the use of 4,5-diazafluoren-9-one (DAF) as an ancillary ligand. Operando XAS and NMR spectroscopic studies provide clear evidence for two kinetic phases, characterized by different catalyst resting states and turnover-limiting steps. The initial burst phase features the formation of an unusual DAF-bridged dimeric Pd^I species, which then evolves into a π-allyl-Pd^{II} catalyst resting state following the burst phase of the reaction. Allylic C–H activation is the rate determining step during the burst phase, while catalyst reoxidation by O_2 is turnover-limiting following the burst. The results described herein provide valuable new insights into this widely studied catalytic reaction, perhaps most importantly shedding light on the contribution of ancillary ligands to key steps in the catalytic mechanism. These insights provide a foundation for the exploration of new ancillary ligands and catalyst designs capable of efficient Pd-catalyzed allylic C–H oxidation.

ASSOCIATED CONTENT

Supporting Information. The Supporting Information is available free of charge on the ACS Publications website: Experimental details and compound characterization data (PDF); Crystallographic data for **3** and **4** (CIF).

AUTHOR INFORMATION

Corresponding Author

*stahl@chem.wisc.edu

Notes
The authors declare no competing financial interests.

ACKNOWLEDGMENT
We would like to thank Dr. Nicholas J. Beach, Mr. Steve Myers and Mr. Kendall Schneider for their assistance in designing and constructing the reactor used at Argonne. Drs. James R. Gallagher and James B. Gerken were instrumental in performing XAS experiments on the beamline. We are grateful to Dr. Kelsey Miles, Dr. Brian Dolinar and Dr. Ilia Guzei for assistance in performing XRD analysis. Drs. Jamie Y. C. Chen and Paul White for insightful discussions. This work was funded by the NSF (CHE-1665120), and builds upon initial work supported by the NIH (R01 GM67173). NMR instrumentation was supported by NSF CHE-1048642, NSF CHE-9709065, NIH S10 OD012245 and a generous gift from Paul J. and Margaret M. Bender. The WiHP-NMRR was supported by the Dow Chemical Company. Use of the Advanced Photon Source is supported by the U.S. Department of Energy, Office of Science, and Office of Basic Energy Sciences, under Contract DE-AC02-06CH11357. MRCAT operations are supported by the Department of Energy and the MRCAT member institutions. C. V. K. was supported in part by the National Science Foundation Graduate Research Fellowship Program under Grant No. DGE-1256259. Any opinions, findings, and conclusions or recommendations expressed in this material are those of the authors and do not necessarily reflect the views of the National Science Foundation. Support was also provided by the Graduate School and the Office of the Vice Chancellor for Research and Graduate Education at the University of Wisconsin-Madison with funding from the Wisconsin Alumni Research Foundation.

References.

1. Smidt, J.; Hafner, W.; Jira, R.; Sedlmeier, J.; Sieber, R.; Ruttinger, R.; Kojer, H. Katalytische Umsetzungen von Olefinen an Platinmetall-Verbindungen. *Angew. Chem.* **1959**, *71*, 176.

2. Vargaftik, M. N.; Moiseev, I. I.; Syrkin, Ya. K. Formation of Mixed Allyl Esters During Reaction of Higher Olefins with Palladium Chloride in Anhydrous Carboxylic Acid Solutions. *Izv. Akad. Nauk SSSR* **1962**, *5*, 930-931.

3. Anderson, C. B.; Winstein, S. Synthesis of the Tricyclo[3.2.1.$0^{3,6}$]octane System. *J. Org. Chem.* **1963**, *28*, 605-606.

4. For a recent review, see: Liron, F.; Oble, J.; Lorion, M. M.; Poli, G. Direct Allylic Functionalization Through Pd-Catalyzed C–H Activation. *Eur. J. Org. Chem.* **2014**, 5863-5883.

5. McMurry, J. E.; Kočovsky, P. A Method for the Palladium-Catalyzed Allylic Oxidation of Olefins. *Tet. Lett.* **1984**, *25*, 4187-4190.

6. Åkermark, B.; Hansson, S. Rein, T.; Vågberg, J.; Heumann, A.; Bäckvall, J.-E. Palladium-Catalyzed Allylic Acetoxylation: an Exploratory Study of the Influence of Added Acids *J. Org. Chem.* **1989**, *369*, 433-444.

7. Chen, M. S.; White, M. C. A Sulfoxide-Promoted, Catalytic Method for the Regioselective Synthesis of Allylic Acetates from Monosubstituted Olefins via C-H Oxidation. *J. Am. Chem. Soc.* **2004**, *126*, 1346-1347.

8. Chen, M. S.; Prabagaran, N.; Labenz, N. A.; White, M. C. Serial Ligand Catalysis: A Highly Selective Allylic C-H Oxidation. *J. Am. Chem. Soc.* **2005**, *127*, 6970-6971.

9. Covell, D. J.; White, M. C. A Chiral Lewis Acid Strategy for Enantioselective Allylic C–H Oxidation. *Angew. Chem. Int. Ed.* **2008**, *47*, 6448- 6451.

10. Lin, B.-L.; Labinger, J. A.; Bercaw, J. E. Mechanistic Investigations of Bipyrimidinepromoted Palladium-Catalyzed Allylic Acetoxylation of Olefins. *Can. J. Chem.* **2009**, *87*, 264-271.

11. Thiery, E.; Aouf, C.; Belloy, J.; Harakat, D.; Le Bras, J.; Muzart, J. Palladium-Catalyzed Allylic Acyloxylation of Terminal Alkenes in the Presence of a Base. *J. Org. Chem.* **2009**, *75*, 1771-1774.

12. Kondo, H.; Yu, F.; Yamaguchi, J.; Liu, G.; Itami, K. Branch-Selective Allylic C−H Carboxylation of Terminal Alkenes by Pd/sox Catalyst. *Org. Lett.* **2014**, *16*, 4212-4215.

13. Malik, H. A.; Taylor, B. L. H.; Kerrigan, J. R.; Grob, J. E.; Houk, K. N.; Du Bois, J.; Hamann, L. G.; Patterson, A. W. Non-Directed Allylic C–H Acetoxylation in the Presence of Lewis Basic Heterocycles. *Chem. Sci.* **2014**, *5*, 2352-2361.

14. Heumann, A.; Reglier, M.; Waegell, B. Oxidation with Palladium Salts: Stereo- and Regiospecific Acetoxylation of 4-Vinylcyclohexene Derivatives. *Angew. Chem. Int. Ed. Engl.* **1982**, *21*, 366-367.

15. Firdoussi, L. E.; Baqqa, A.; Allaoud, S.; Allal, B. A.; Karim, A.; Catanet, Y.; Mortreux, A. Selective Palladium-Catalysed Functionalization of Limonene: Synthetic and Mechanistic aspects. *J. Mol. Catal. A: Chem.* **1998**, *135*, 11-22.

16. Jia, C.; Müller, P.; Mimoun, H. Palladium-Catalyzed Allylic Acetoxylation of Olefins Using Hydrogen Peroxide as Oxidant. *J. Mol. Catal. A: Chem.* **1995**, *101*, 127-136.

17. Pilarski L. T.; Janson, P. G.; Szabó, K. J. Palladium-Catalyzed Selective Acyloxylation Using Sodium Perborate as Oxidant. *J. Org. Chem.* **2011**, *76*, 1503-1506.

18. Xing, X.; O'Connor, N. R.; Stoltz, B. M. Palladium(II)-Catalyzed Allylic C–H Oxidation of Hindered Substrates Featuring Tunable Selectivity Over Extent of Oxidation. *Angew. Chem. Int. Ed.* **2015**, *54*, 11186-11190.

19. Litman, Z. C.; Sharma, A.; Hartwig, J. F. Oxidation of Hindered Allylic C−H Bonds with Applications to the Functionalization of Complex Molecules. *ACS Catal.* **2017**, *7*, 1998-2001.

20. Pilarski L. T.; Selander, N.; Bose, D.; Szabó, K. J. Catalytic Allylic C-H Acetoxylation and Benzoyloxylation via Suggested (η^3-Allyl)palladium(IV) Intermediates. *Org. Lett.* **2009**, *11*, 5518-5521.

21. Alam, R.; Pilarski L. T.; Pershagen, E.; Szabó, K. J. Stereoselective Intermolecular Allylic C−H Trifluoroacetoxylation of Functionalized Alkenes. *J. Am. Chem. Soc.* **2012**, *134*, 8778-8781.

22. Bäckvall, J. E.; Hopkins, R. B.; Grennberg, H.; Mader, M. M.; Awasthi, A. K. Multistep Electron Transfer in Palladium-Catalyzed Aerobic Oxidations via a Metal Macrocycle-Quinone System. *J. Am. Chem. Soc.* **1990**, *112*, 5160-5166.

23. Hansson, S.; Heumann, A.; Rein, T. Åkermark, B. Preparation of Allylic Acetates from Simple Alkenes by Palladium(I1)-Catalyzed Acetoxylation. *J. Org. Chem.* **1990**, *55*, 975-984.

24. Larsson, E. M.; Akermark, B. A Catalytic System for Allylic Acetoxylation Consisting of Palladium(II) and Nitrate and Using Oxygen as Final Oxidant. *Tet. Lett*. **1993**, *34*, 2523-2526.

25. Principato, B.; Maffei, M.; Siv, C.; Buono, G.; Peiffer, B. Palladium Catalysed Allylic Acetoxylation of Dialkyl Allyl Phosphonates. *Tetrahdron*, **1996**, *52*, 2087-2096.

26. Gusevskaya, E.; Gonsalves, J. A. Palladium(II) Catalyzed Oxidation of Naturally Occurring Terpenes with Dioxygen. *J. Mol. Catal. A: Chem.* **1997**, *121*, 131-137.

27. Henderson, W. H.; Check, C. T.; Proust, N.; Stambuli, J. P. Allylic Oxidations of Terminal Olefins Using a Palladium Thioether Catalyst. *Org. Lett.* **2010**, *12*, 824-827.

28. Thiery, E.; Aouf, C.; Belloy, J.; Harakat, D.; Le Bras, J.; Muzart, J. Palladium-Catalyzed Allylic Acyloxylation of Terminal Alkenes in the Presence of a Base. *J. Org. Chem.* **2010**, *75*, 1771-1774.

29. For a review of oxidation cocatalyst systems employing redox mediators in reactions beyond Pd-catalyzed oxidations, see: Piera, J.; Bäckvall, J. Catalytic Oxidation of Organic Substrates by Molecular Oxygen and Hydrogen Peroxide by Multistep Electron Transfer—A Biomimetic Approach. *Angew. Chem. Int. Ed.* **2008**, *47*, 3506-3523.

30. Mitsudome, T.; Umetani, T.; Nosaka, N.; Mori, K.; Mizugaki, T.; Ebitani, K.; Kaneda, K. Convenient and Efficient Pd-Catalyzed Regioselective Oxyfunctionalization of Terminal Olefins by Using Molecular Oxygen as Sole Reoxidant. *Angew. Chem. Int. Ed.* **2006**, *45*, 481-485.

31. Campbell, A. N.; White, P. B.; Guzei, I. A.; Stahl S. S. Allylic C-H Acetoxylation with a 4,5-Diazafluorenone-Ligated Palladium Catalyst: A Ligand-Based Strategy To Achieve Aerobic Catalytic Turnover. *J. Am. Chem. Soc.* **2010**, *132*, 15116-15119.

32. Fraunhoffer, K. J.; Prabagaran, N.; Sirois, L. E.; White, M. C. Macrolactonization via Hydrocarbon Oxidation. *J. Am. Chem. Soc.* **2006**, *128*, 9032 – 9033.

33. Stang, E. M.; White, M. C. Total Synthesis and Study of 6-Deoxyerythronolide B by Late-Stage C–H Oxidation. *Nat. Chem.* **2009**, *1*, 547-551.

34. Vermeulen, N. A.; Delcamp, J. H.; White, M. C. Synthesis of Complex Allylic Esters via C–H Oxidation vs C–C Bond Formation. *J. Am. Chem. Soc.* **2010**, *132*, 11323-11328.

35. Trost, B. M.; Thaisrivongs, D. A.; Donckele, E. J. Palladium-Catalyzed Enantioselective Allylic Alkylations through C–H Activation. *Angew. Chem. Int. Ed.* **2013**, *52*, 1523-1526.

36. Wang, P.-S.; Liu, P.; Zhai, Y.-J.; Lin, H.-C.; Han, Z.-Y.; Gong, L.-Z. Asymmetric Allylic C−H Oxidation for the Synthesis of Chromans. *J. Am. Chem. Soc.* **2015**, *137*, 12732-12735.

37. Amman, S. E.; Liu, W.; White, M. C. Enantioselective Allylic C–H Oxidation of Terminal Olefins to Isochromans by Palladium(II)/Chiral Sulfoxide Catalysis. *Angew. Chem. Int. Ed.* **2016**, *55*, 9571-9575.

38. Gormisky, P. E.; White, M. C. Synthetic Versatility in C–H Oxidations: A Rapid Approach to Differentiated Diols and Pyrans from Simple Olefins. *J. Am. Chem. Soc.* **2011**, *133*, 12584-12589.

39. For discussion of ligand effects on Pd-catalyzed aerobic oxidation reactions, see the following and refs. 40 and 41: Stahl, S. S. Palladium Oxidase Catalysis: Selective Oxidation

of Organic Chemicals by Direct Dioxygen-Coupled Turnover. *Angew. Chem. Int. Ed*. **2004***, 43*, 3400-3420.

40. Gligorich, K. M.; Sigman, M. S. Recent Advancements and Challenges of Palladium^{II}-Catalyzed Oxidation Reactions with Molecular Oxygen as the Sole Oxidant. *Chem. Commun*. **2009**, 3854-3867.

41. Wang, D.; Weinstein, A. B.; White, P. B.; Stahl, S. S. Ligand-Promoted Palladium-Catalyzed Aerobic Oxidation Reactions. *Chem. Rev.* **2018**, *118*, 2636-2679.

42. Amatore, C.; Jutand, A. Mechanistic and Kinetic Studies of Palladium Catalytic Systems. *J. Organomet. Chem.* **1999**, *576*, 254-278.

43. *Metal-Catalyzed Cross-Coupling Reactions*. de Meijere, A.; Diederich, F., Eds.; Wiley-VCH, Weinheim, 2004, and references therein.

44. Blackmond, D. G. Reaction Progress Kinetic Analysis: A Powerful Methodology for Mechanistic Studies of Complex Catalytic Reactions. *Angew. Chem. Int. Ed.* **2005**, *44*, 4302-4320.

45. Hartwig, J. F. Carbon-heteroatom Bond Formation Catalyzed by Organometallic Complexes. *Nature* **2008**, *455*, 314-322.

46. Rosner, T.; LeBars, J.; Pfaltz, A.; Blackmond, D. G. Kinetic Studies of Heck Coupling Reactions Using Palladacycle Catalysts: Experimental and Kinetic Modeling of the Role of Dimer Species. *J. Am. Chem. Soc.* **2001**, *123*, 1848-1855.

47. Alvaro, E.; Hartwig, J. F. Resting State and Elementary Steps of the Coupling of Aryl Halides with Thiols Catalyzed by Alkylbisphosphine Complexes of Palladium. *J. Am. Chem. Soc.* **2009**, *131*, 22, 7858-7868.

48. Seechurn, C. C. C. J.; Sperger, T.; Scrase, T. G.; Schoenebeck, F.; Colacot, T. J. Understanding the Unusual Reduction Mechanism of Pd(II) to Pd(I): Uncovering Hidden Species and Implications in Catalytic Cross-Coupling Reactions. *J. Am. Chem. Soc.*, **2017**, *139,* 5194-5200.

49. Surry, D. S.; Buchwald, S. L. Biaryl Phosphane Ligands in Palladium-Catalyzed Amination. *Angew. Chem. Int. Ed.* **2008**, *47*, 6338-6361.

50. Fortman, G. C.; Nolan, S. P. *N*-Heterocyclic Carbene (NHC) Ligands and Palladium in Homogeneous Cross-Coupling Catalysis: A Perfect Union. *Chem. Soc. Rev.* **2011**, *40*, 5151-5169.

51. Valente, C.; Pompeo, M.; Sayah, M.; Organ, M. G. Carbon−Heteroatom Coupling Using Pd-PEPPSI Complexes. *Org. Process Res. Dev.* **2014**, *18*, 180-190.

52. Hazari, N.; Hruszkewycz, D. P. Dinuclear Pd^{I} Complexes with Bridging Allyl and Related Ligands. *Chem. Soc. Rev.* **2016**, *45*, 2871–2899.

53. Gildner, P. G.; Colacot, T. J. Reactions of the 21st Century: Two Decades of Innovative Catalyst Design for Palladium-Catalyzed Cross-Couplings. *Organometallics* **2015**, *34*, 5497-5508.

54. Littke, A. F.; Fu, G. C. Palladium-Catalyzed Coupling Reactions of Aryl Chlorides. *Angew. Chem. Int. Ed.* **2002**, *41*, 4176-4211.

55. White, P. B.; Jaworski, J. N.; Fry, C. G.; Dolinar, B. S.; Guzei, I. A.; Stahl, S. S. Structurally Diverse Diazafluorene-Ligated Palladium(II) Complexes and Their Implications for Aerobic Oxidation Reactions. *J. Am. Chem. Soc.* **2016**, 138, 4869-4880.

56. For a review of the rich DAF coordination chemistry with various transition metals, see: Annibale, V. T.; Song, D. Coordination Chemistry and Applications of Versatile 4,5-Diazafluorene Derivatives. *Dalton Trans.* **2016**, *45*, 32-49.

57. For simplicity, the term "reductive elimination" is applied to the step generating allyl acetate from the allyl-Pd^{II} intermediate. Although the mechanism of this reaction could proceed via inner-sphere or outer-sphere attack of an acetate on the allyl ligand, both pathways result in the "reduction" of Pd^{II} to Pd^{0} and the "elimination" of allyl acetate as the product. For context, similar usage of the term "reductive elimination" is applied to the formation of C–X bonds from d^6 octahedral metal complexes, even when the C–X bond is formed via outer-sphere attack of the nucleophile. See, for example: Williams, B. S.; Goldberg, K. I. Studies of Reductive Elimination Reactions To Form Carbon-Oxygen Bonds from Pt(IV) Complexes. *J. Am. Chem. Soc.* **2001**, *123*, 2576-2587.

58. Diao, T.; Stahl, S. S. O_2-Promoted Allylic Acetoxylation of Alkenes: Assessment of ‘‘Push’’ versus ‘‘Pull’’ Mechanisms and Comparison Between O_2 and Benzoquinone. *Polyhedron* **2014**, *84*, 96-102.

59. The beneficial effect of DAF has been demonstrated in a number of Pd-catalyzed oxidation reactions beyond allylic oxidation. See references 60-69.

60. White, P. B.; Jaworski, J. N.; Geyunjian, H. Z.; Stahl, S. S. Diazafluorenone-Promoted Oxidation Catalysis: Insights into the Role of Bidentate Ligands in Pd-Catalyzed Aerobic Aza-Wacker Reactions. *ACS Catal.* **2016**, *6*, 3340-3348.

61. Campbell, A. N.; Meyer, E. B.; Stahl, S. S. Regiocontrolled Aerobic Oxidative Coupling of Indoles and Benzene using Pd Catalysts with 4,5-Diazafluorene Ligands. *Chem. Commun.* **2011**, *47*, 10257-10259.

62. Xia, B.; Gong, T. J.; Liu, Z.-J.; Liu, J.-H.; Luo, D.-F.; Xu, J.; Liu, L. Synthesis of Dibenzofurans via Palladium-Catalyzed Phenol-Directed C–H Activation/C–O Cyclization. *J. Am. Chem. Soc.* **2011**, *133*, 9250-9253.

63. Piotrowicz, M.; Zakrzewski, J. Aerobic Dehydrogenative Heck Reaction of Ferrocene with a $Pd(OAc)_2$/4,5-Diazafluoren-9-one Catalyst. *Organometallics* **2013**, *32*, 5709-5712.

64. Piotrowicz, M.; Zakrewski, Métivier, R.; Brosseau, A.; Makal, A.; Woźniak, K. Aerobic Palladium(II)-Catalyzed Dehydrogenative Heck Reaction in the Synthesis of Pyrenyl Fluorophores. A Photophysical Study of β-Pyrenyl Acrylates in Solution and in the Solid State. *J. Org. Chem.* **2015**, *80*, 2573-2581.

65. Vasseur, A.; Laugel, C.; Harakat, D.; Muzart, J.; Le Bras, J. Ligand-Promoted Reactivity of Alkenes in Dehydrogenative Heck Reactions of Furans and Thiophenes. *Eur. J. Org. Chem.* **2015**, *5*, 944–948.

66. Kim, H. T.; Ha, H.; Kang, G.; Kim, O. S.; Ryu, H.; Biswas, A. K.; Lim, S. M.; Baik, M.-H.; Joo, J. M. Ligand-controlled Regiodivergent C–H Alkenylation of Pyrazoles and its Application to the Synthesis of Indazoles. *Angew. Chem. Int. Ed.* **2017**, *56*, 16262-16266.

67. Gao, W. M.; He, Z. Q.; Qian, Y.; Zhao, J.; Huang, Y. General Palladium-Catalyzed Aerobic Dehydrogenation to Generate Double Bonds. *Chem. Sci.* **2012**, *3*, 883-886.

68. Diao, T.; Wadzinski, T. J.; Stahl, S. S. Direct Aerobic α,β-Dehydrogenation of Aldehydes and Ketones with a $Pd(TFA)_2$/4,5-Diazafluorenone Catalyst. *Chem. Sci.* **2012**, *3*, 887-891.

69. Buter, J.; Moezelaar, R.; Minnaard, A. J. Enantioselective Palladium Catalyzed Conjugate Additions of Ortho-Substituted Arylboronic Acids to β,β-Disubstituted Cyclic Enones: Total Synthesis of Herbertenediol, Enokipodin A and Enokipodin B. *Org. Biomol. Chem.* **2014**, *12*, 5883-5890.

70. Jaworski, J. N.; McCann, S. D.; Guzei, I. A.; Stahl, S. S. Detection of Palladium(I) in Aerobic Oxidation Catalysis. *Angew. Chem. Int. Ed.* **2017**, *56*, 3605-3610.

71. High yields of product formation (>40% yield) could not be obtained at 60 °C, the previously reported optimized reaction temperature, but were possible at 80 °C. Therefore, kinetic investigations were generally performed at 80 °C.

72. Nelson, R. C.; Miller, J. T. An Introduction to X-ray Absorption Spectroscopy and its *in situ* Application to Organometallic Compounds and Homogeneous Catalysts. *Catal. Sci. Tech.* **2012**, *2*, 461-470.

73. Sherborne, G. J.; Nguyen, B. N. Recent XAS studies into Homogeneous Metal Catalyst in Fine Chemical and Pharmaceutical Syntheses. *Chem. Cent. J.* **2015**, *9*, 37.

74. For other representative applications of XAS to the analysis of molecular Pd complexes and Pd-catalyzed reactions, see the following and refs. 75-79: Evans, J.; O'Neill, L.; Kambhampati, V. L.; Rayner, G.; Turin, S.; Genge, A.; Dent, A. J.; Neisius, T. Structural Characterisation of Solution Species Implicated in the Palladium-Catalysed Heck Reaction by Pd K-edge X-ray Absorption Spectroscopy: Palladium Acetate as a Catalyst Precursor. *Dalton Trans.* **2002**, 2207-2212.

75. Tromp, M.; Sietsma, J. R. A.; van Bokhoven, J. A.; van Strijdonck, G. P. F.; van Haaren, R. J.; van der Eerden, A. M. J.; van Leeuwen, P. W. N. M; Koningsberger, D. C. Deactivation

Processes of Homogeneous Pd Catalysts using *in situ* Time Resolved Spectroscopic Techniques. *Chem. Commun.* **2003**, 128-129.

76. Fiddy, S. G.; Evans, J.; Newton, M. A.; Neisius, T.; Tooze, R. P.; Oldman, R. Extended X-ray Absorption Fine Structure (EXAFS) Characterisation of Dilute Palladium Homogeneous Catalysts. *Chem. Commun.* **2003**, 2682-2683.

77. Tromp, M.; van Bokhoven, J. A.; van Strijdonck, G. P. F.; van Leeuwen, P. W. N. M.; Koningsberger, D. C.; Ramaker, D. E. Probing the Molecular Orbitals and Charge Redistribution in Organometallic (PP)Pd(XX) Complexes. A Pd K-Edge XANES Study. *J. Am. Chem. Soc.* **2005,** *127*, 777-789.

78. Fiddy, S. G.; Evans, J.; Neisius, T.; Newton, M. A.; Tsoureas, N.; Tulloch, A. A. D.; Danopoulos, A. A. Comparative Experimental and EXAFS Studies in the Mizoroki–Heck Reaction with Heteroatom-Functionalised N-Heterocyclic Carbene Palladium Catalysts. *Chem. Eur. J.* **2007**, *13*, 3652-3659.

79. MacMillan, S. N.; Lancaster, K. M. X-ray Spectroscopic Interrogation of Transition-Metal-Mediated Homogeneous Catalysis: Primer and Case Studies. *ACS Catal.* **2017**, *7*, 1776-1791.

80. Tereniak, S. J.; Stahl, S. S. Mechanistic Basis for Efficient, Site-Selective, Aerobic Catalytic Turnover in Pd-Catalyzed C−H Imidoylation of Heterocycle- Containing Molecules. *J. Am. Chem. Soc.* **2017**, *139*, 14533-14541.

81. Reaction conditions for the operando XANES study: [$Pd(OAc)_2$] = [DAF] = 13.5 mM, [NaOAc] = 54 mM, [allylbenzene] = 0.27 M, total reaction mixture was 3 mL in 3:1 dioxane/AcOH. The reaction was run at 80 °C with a stir rate of 700 rpm. O_2 was provided

via a balloon using a custom PEEK cell (details in Supporting Information). Spectra were acquired from the region of 24.1 keV to 25.1 keV with a frequency of approximately 0.4 eV.

82. Previous high-pressure NMR experiments in the Stahl group have been performed using J-Young tubes and condensing known amount of O_2 with liquid nitrogen. See refs. 83-84 for pertinent examples. However, a safer and easier method was realized using components available from Wilmad-Labglass. These experiments are only adequate for studying the beginning phase of the reaction as there is not a mechanism for mixing the reaction solution and replenishing consumed O_2 using static tubes. Deconvoluting mass-transport phenomena from chemical reaction kinetics can become challenging at extended time points. See supporting information for additional details.

83. Steinhoff, B. A.; Guzei, I. A.; Stahl S. S. Mechanistic Characterization of Aerobic Alcohol Oxidation Catalyzed by $Pd(OAc)_2$/Pyridine Including Identification of the Catalyst Resting State and the Origin of Nonlinear [Catalyst] Dependence. *J. Am. Chem. Soc.* **2004**, *126*, 11268-11278.

84. Ye, X.; Liu, G.; Popp, B. V.; Stahl, S. S. Mechanistic Studies of Wacker-Type Intramolecular Aerobic Oxidative Amination of Alkenes Catalyzed by $Pd(OAc)_2$/Pyridine. *J. Org. Chem.* **2011**, *76*, 1031-1044.

85. Beach, N. J.; Knapp, S. M. M.; Landis, C. R. A Reactor for High-Throughput High-Pressure Nuclear Magnetic Resonance Spectroscopy. *Rev. Sci. Instrum.* **2015**, *86*, 104101.

86. Chotchatchawankul, S., Mechanistic Studies of Rh(diphosphine)-Catalyzed Methanol Reductive Carbonylation, Dissertation, University of Wisconsin - Madison. Madison, WI, 2015.

87. Brezny, A. C.; Landis, C. R. Unexpected CO Dependencies, Catalyst Speciation, and Single Turnover Hydrogenolysis Studies of Hydroformylation via High Pressure NMR Spectroscopy. *J. Am. Chem. Soc.* **2017**, *139*, 2778-2785.

88. A gas mixture of 9% O_2 in N_2 was used to mitigate flammability concerns, and a sapphire NMR tube allowed for the use of high gas pressures. For discussion of O_2 flammability limits, see: Osterberg, P. M.; Niemeier, J. K.; Welch, C. J.; Hawkins, J. M.; Martinelli, J. R.; Johnson, T. E.; Root, T. W; Stahl, S. S. Experimental Limiting Oxygen Concentrations for Nine Organic Solvents at Temperatures and Pressures Relevant to Aerobic Oxidations in the Pharmaceutical Industry. *Org. Process Res. Dev.* **2015**, *19*, 1537-1543.

89. Knapp, S. M. M.; Shaner, S. E.; Kim, D.; Shopov, D. Y.; Tendler, J. A.; Pudalov, D. M.; Chianese, A. R. Mechanistic Studies of Alkene Isomerization Catalyzed by CCC-Pincer Complexes of Iridium. *Organometallics* **2014**, *33*, 473-484.

90. Yin, G.; Wu, Y.; Liu, G. Scope and Mechanism of Allylic C–H Amination of Terminal Alkenes by the Palladium/PhI(OPiv)$_2$ Catalyst System: Insights into the Effect of Naphthoquinone. *J. Am. Chem. Soc.* **2010**, *132*, 11978-11987.

91. Powell, J.; Robinson, S. D.; Shaw, B. L. Intermediates in the Conversion of π- into σ-Allylic Palladium(II) Complexes. *Chem. Commun. (London)* **1965**, *0*, 78-79.

92. Powell, J.; Shaw, B. L. Transition Metal-Carbon Bonds. Part X. Reactions between Allylic Palladium Halides and Tertiary Phosphines, Triphenylarsine, Triphenylstibine, or Carbon Monoxide. *J. Chem. Soc. A* **1967**, *0*, 1839-1851.

93. Jalón, F. A.; Manzano, B. R.; Otero, A.; Rodríguez-Pérez, M. C. Synthesis and Fluxional Behaviour of Allylpalladium Complexes with Poly(pyrazol-1-yl)methane Ligands. *J. Organomet. Chem.* **1995**, *494*, 179-185.

94. Engelin, C.; Jensen, T.; Rodriguez-Rodriguez, S.; Fristrup, P. Mechanistic Investigation of Palladium-Catalyzed Allylic C−H Activation. *ACS Catal.* **2013**, *3*, 294-302.

95. Gómez-Gallego, M.; Sierra, M. A. Kinetic Isotope Effects in the Study of Organometallic Reaction Mechanisms. *Chem. Rev.* **2011**, *111*, 4857-4963.

96. Bonney, K. J.; Schoenebeck, F. Experiment and Computation: a Combined Approach to Study the Reactivity of Palladium Complexes in Oxidation States 0 to IV. *Chem. Soc. Rev.* **2014**, *43*, 6609-6638.

97. Xu, Q.; Souma, Y.; Umezawa, J.; Tanaka, M.; Nakatani, H. Palladium(I) Carbonyl Cation-Catalyzed Carbonylation of Olefins and Alcohols in Concentrated Sulfuric Acid. *J. Org. Chem.* **1999**, *64*, 6306-6311.

98. Temkin, O. N.; Bruk, L. G. Palladium(II, I, 0) Complexes in Catalytic Reactions of Oxidative Carbonylation. *Kinet. Catal*. **2003**, *44*, 601-617.

99. Stromnova, T. A. Palladium(+1) Carbonyl Clusters in the Catalytic Oxidation of Unsaturated Compounds. *Platinum Met. Rev.* **2003**, *47*, 20-27.

100. Ragaini, F.; Larici, H.; Rimoldi, M.; Caselli, A.; Ferretti, F.; Maachi, P.; Casati, N. Mapping Palladium Reduction by Carbon Monoxide in a Catalytically Relevant System. A Novel Palladium(I) Dimer. *Organometallics* **2011**, *30*, 2385-2393.

101. Toledo, A.; Funes-Ardoiz, I.; Maseras, F.; Albéniz, A. C. Palladium-Catalyzed Aerobic Homocoupling of Alkynes: Full Mechanistic Characterization of a More Complex Oxidase-Type Behavior. *ACS Catal.* **2018**, *8*, 7495–7506.

102. For an example of direct reactivity between O_2 and a Pd^I dimer, see: Huacuja, R.; Graham, D. J.; Fafard, C. M.; Chen, C.-H.; Foxman, B. M.; Herbert, D. E.; Alliger, G.; Thomas, C. M.; Ozerov, O. V. Reactivity of a Pd(I)–Pd(I) Dimer with O_2: Mohohapto Pd Superoxide and Dipalladium Peroxide in Equilibrium. *J. Am. Chem. Soc.* **2011**, *13*, 3820-3823.

103. Pd-catalyzed aerobic oxidation reactions rarely exhibit a kinetic dependence on pO_2 and precedents typically arise from mass-transport limitations. In the present reaction, mass transport limitations may be ruled out on the basis of the increase in rate with higher [catalyst] and [allylbenzene]. If the O_2 dependence reflected mass-transport limitations, the reaction rate should reach a plateau with a sharp break at higher [catalyst] and [allylbenzene], reflecting the O_2 mass transport rate (cf. data for the oxidative amidation reaction in ref. 70). For another example of a Pd-catalyzed aerobic oxidation reaction that exhibits a positive order in pO_2, see ref. 101.

104. Steinhoff, B. A.; Stahl, S. S. Mechanism of $Pd(OAc)_2$/DMSO-Catalyzed Aerobic Alcohol Oxidation: Mass-Transfer-Limitation Effects and Catalyst Decomposition Pathways. *J. Am. Chem. Soc.* **2006**, *128*, 4348-4355.

105. Stahl, S. S.; Thorman, J. L.; Nelson, R. C.; Kozee, M. A. Oxygenation of Nitrogen-Coordinated Palladium(0): Synthetic, Structural, and Mechanistic Studies and Implications for Aerobic Oxidation Catalysis. *J. Am. Chem. Soc.* **2001**, *123*, 7188-7189.

106. Popp, B. V.; Stahl, S. S. "Oxidatively Induced" Reductive Elimination of Dioxygen from an η^{2}-Peroxopalladium(II) Complex Promoted by Electron-Deficient Alkenes. *J. Am. Chem. Soc.* **2006**, 128, 2804-2805.

107. Popp, B. V.; Morales, C. M.; Landis, C. R.; Stahl, S. S. Electronic Structural Comparison of the Reactions of Dioxygen and Alkenes with Nitrogen-Chelated Palladium(0). *Inorg. Chem.* **2010**, 49, 8200-8207.

108. Bäckvall, J.-E.; Gogoll, A. Evidence for (π-allyl)Palladium(II)(quinone) Complexes in the Palladium-Catalyzed 1,4-Diacetoxylation of Conjugated Dienes. *Tetrahedron Lett.* **1988**, *29*, 2243-2246.

109. Grennber, H.; Gogoll, A.; Bäckvall, J.-E. Use of Sulfoxides as Cocatalysts in the Palladium-Quinone-Catalyzed l,4-Diacetoxylation of 1,3-Dienes. An Example of Ligand-Accelerated Catalysis. *J. Org. Chem.* **1991**, *56*, 5808-5811.

TOC Graphic

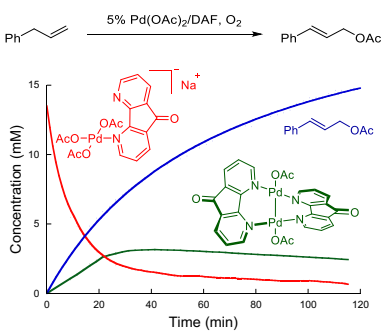

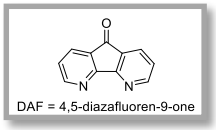

- Ligand supported aerobic catalytic turnover
- Rapid burst of product formation followed by steady state
- Transient formation of dimeric Pd(I) species